1998

Studies on Electroless Cobalt Coatings for Microencapsulation of Hydrogen Storage Alloys

Bala S. Haran
University of South Carolina - Columbia

Branko N. Popov
University of South Carolina - Columbia, popov@engr.sc.edu

Ralph E. White
University of South Carolina - Columbia, white@cec.sc.edu

Publication Info

Journal of the Electrochemical Society, 1998, pages 3000-3007.

Publisher's link: http://dx.doi.org/10.1149/1.1838754
DOI: 10.1149/1.1838754

Studies on Electroless Cobalt Coatings for Microencapsulation of Hydrogen Storage Alloys

Bala S. Haran,* Branko N. Popov,* and Ralph E. White*

Department of Chemical Engineering, University of South Carolina, Columbia, South Carolina 29208, USA

ABSTRACT

$LaNi_{4.27}Sn_{0.24}$ alloy was microencapsulated with cobalt by electroless deposition from an alkaline hypophosphite bath. Discharge curves of the encapsulated alloy indicate an additional contribution to the capacity arising from the cobalt on the surface. Studies on cobalt thin films reveal the presence of adsorbed hydrogen in cobalt. The amount of hydrogen adsorbed was observed to increase with time of cathodic polarization and to reach a maximum. Polarization techniques have been used to characterize the cobalt-plated alloy as a function of state of charge. The equilibrium potential of the microencapsulated electrode at low hydrogen concentration is determined by the potential of the cobalt coating on the surface.

Introduction

Nickel hydride batteries (MH) with reversible hydrogen storage alloys have recently attracted great attention. For practical electrochemical devices, metal hydrides are sought with the following properties: high capacity to store hydrogen, low hydrogen equilibrium pressure, high rates of absorption and desorption, long cycle life, low cost, light weight, and corrosion resistance.[1] Although some of these properties have been achieved by the optimization of alloy composition for stability and hydrogen reversibility, challenges remain in the form of capacity decay and corrosion resistance for the development of an efficient NiOOH–metal hydride (Ni-MH) cell.[2]

Capacity decay arises because of alloy pulverization and subsequent oxidation of the hydride surface during repeated charge–discharge cycles. During cycling of the electrodes, precipitates of metals are produced at the surface by segregation and decomposition[3,4] of active material. X-ray photoelectron spectroscopy (XPS) depth profiles of $LaNi_5$ by Schlapbach et al.[3] and $MmNi_{3.45}(CoMnTi)_{1.55}$ by Lei et al.[4] reveal an oxygen-enriched and nickel-deficient surface layer. For both AB_2- and AB_5-type hydrides, the only faradaic reaction involved during discharge is the desorption of hydrogen from the material. However, if additional faradaic reactions are involved these would only increase the capacity. It is desirable to have a material which gives high energy densities. It has been shown that microencapsulation provides increased oxidation resistance of the alloy surface improved adherence, and better electrical and thermal conductivities during cycling.[5-8]

Microencapsulation is the process of electroless plating of alloy particles with a thin layer of copper,[5] nickel,[6,7] or palladium.[8] The coatings lead to superior electrodes, with a constant capacity and longer cycle life compared to those made with bare alloys. Plating these materials results in decreasing the energy density based on the actual weight of the electrode (alloy + coating + binders). Cobalt coating, in addition to providing the advantages of microencapsulation, also increases the capacity. In spite of the extensive literature on various coatings, none of the studies have focused on the utility of electroless cobalt deposition for microencapsulation of metal hydrides. Partial substitution of Co[9] for nickel in AB_5-type alloys has been found to be beneficial in reducing the volume expansion during hydriding of the alloy. Beneficial $Co(OH)_2$ is formed on the surface during extended cycling.[10] Weizhong et al.[11] found that mixing cobalt powders with $MmNi_{3.9}Cu_{0.4}Al_{0.7}$ alloy resulted in an improvement of the cycle life and a slight increase in the electrochemical capacity of the electrode. An increase in the discharge capacity accompanied by an increased high-rate dischargeability was seen for mixing cobalt oxides (Co_3O_4) with $MmNi_{3.6}Mn_{0.4}Al_{0.3}Co_{0.7}$ particles by Iwakura et al.[12] Ikeya et al.[13] studied the performance of $MmNi_{3.5}Al_{0.8}Co_{0.7}$ mixed with cobalt powder by a mechanical treatment. They found that the formation of a cobalt compound on the surface enhanced the cyclic durability and the discharge capacity of the metal hydride anodes. It can be clearly seen that the presence of cobalt in the electrode, either through substitutions in the alloy or by mixing with the particles, had a beneficial effect on the electrode performance.

The objective of this work has been to study the effect of cobalt microencapsulation on the performance of the hydride electrode. Similar to mixing cobalt powders[11,13] or cobalt oxides[12] with the alloy, an increase in the electrochemical capacity is seen due to the cobalt microencapsulation. Previous investigators have ascribed this to the oxidation of cobalt present.[11,12] The feasibility of this reaction being reversible has not been considered and needs to be explored further. Hence the specific objectives of our research are: (*i*) to microencapsulate metal hydride alloys with thin films of cobalt, (*ii*) to investigate if the oxidation process is reversible so that the oxides/hydroxides formed can be reduced to the original cobalt, and finally (*iii*) to determine the kinetic and thermodynamic parameters of cobalt-plated $LaNi_{4.27}Sn_{0.24}$ alloy as a function of electrode state of charge.

Experimental

$LaNi_{4.27}Sn_{0.24}$ alloys was crushed, ground mechanically, and passed through 170 and 230 mesh sieves to get a particle size of 63–90 μm. Prior to cobalt electroless deposition, the alloy was initially sensitized by immersing in acidified $SnCl_2$ and subsequently activated in acidified $PdCl_2$ aqueous solution. The deposition was carried out with moderate stirring at 80–85°C in 20 g/L cobalt sulfate, 20 g/L sodium hypophosphite, 50 g/L sodium citrate, and 40 g/L ammonium chloride[14] for 1 h. In addition to these constituents, NH_4OH was added periodically during deposition to maintain the pH between 8.5 and 9.5. The pH frequently dropped below 9 during deposition, indicating that cobalt deposition on the alloy surface was proceeding. The deposition was terminated once the pH remained constant, indicating the absence of cobalt in the solution. The alloy powder was rinsed with deionized water, filtered, and dried at 65°C for 12 h. The alloy is magnetic because of the cobalt coating on the surface. From volumetric titrations[14] the cobalt encapsulation was determined to be 28% by weight. Figure 1a and b present the energy-dispersive spectroscopy (EDAX) of the $LaNi_{4.27}Sn_{0.24}$ alloy before and after microencapsulation. From the relative peaks of different elements obtained by EDAX analysis, the bare alloy reveals a weight percent of 67% Ni, 30% La, and 3% of Sn. These atom percent values normalized to 100 are 82% Ni, 16% La, and 2% Sn. These atomic percent values closely correspond to the calculated values of 78% Ni, 18% La, and 4% Sn for the alloy. A small additional

* Electrochemical Society Active Member.

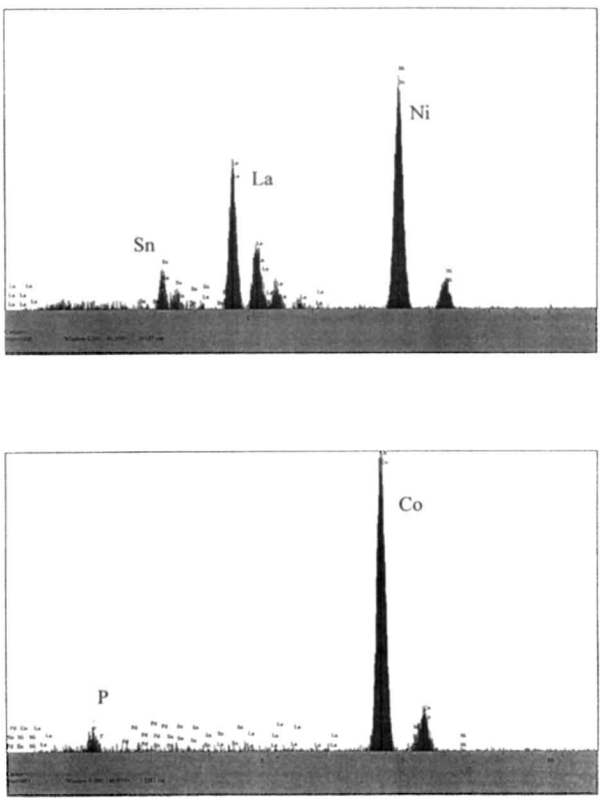

Fig. 1. EDAX analysis of $LaNi_{4.27}Sn_{0.24}$ alloy before (a, top) and after (b, bottom) cobalt plating. The coating is predominantly Co with a small amount of phosphorus, as seen by the peak at 2 μm.

peak of phosphorus was visible for the coated alloy at a wavelength of 2 μm in Fig. 1b. The phosphorus in the coating arises due to the hypophosphite reducing agent present in the bath. From the relative peak heights, we get a weight percent of 94% Co, 3% P, 1.7% Ni, 0.8% La, and 0.5% Sn. Since EDAX looks at the surface of the alloy (to a depth in the order of a few microns), we can conclude that the particles are completely encased with cobalt. An electrode was prepared by mixing the alloy with 2.5 wt % poly(tetrafluoroethylene) (PTFE) followed by hot-pressing the material between two nickel meshes at 300°C and 5 tons/cm^2 in a cylindrical press. A pellet of 0.7 cm diam, 0.60 mm thick, and weight 450 mg was obtained.

Characterization studies were done in a three-electrode setup. The working pellet electrode was inserted between two pieces of Plexiglas and immersed in the cell filled with 6 M KOH solution. All potentials are with respect to the Hg/HgO reference electrode. The counter electrode is a nickel electrode. The cell was maintained at a constant temperature of 25°C using a water bath. A Bitrode model LCN automated cycle life tester was used for cycling the electrode. Electrochemical studies were done using the model 352 SoftCorr System with an EG&G Princeton Applied Research potentiostat/galvanostat model 273. Initially the electrode was charged at a constant current of 3 mA for 12 h and then discharged at 3 mA until the potential reached a cutoff value of −0.6 V. These charge–discharge cycles were repeated ten times in order to activate the electrode.

After conditioning the electrode, state-of-charge (SOC) studies were performed to determine the electrode characteristics. Here, the SOC is defined with respect to the total useful capacity, which includes contributions from both the alloy and cobalt. This capacity was determined from the total time taken to discharge the pellet to −0.6 V at a constant rate of 0.1 C. The active material was discharged for a fixed amount of time at the 0.1 C rate. The SOC was determined from the ratio of the time discharged to the time required for complete discharge. Once the alloy was discharged to a particular SOC, the electrode was left on open circuit until a stable potential was observed (typically between 45 and 60 min). After the potential stabilized, polarization studies were performed. The potential was varied 20 mV above and below the equilibrium potential at a scan rate of 1 mV/s and the current response was measured. The electrode was stable during the measurements and its open-circuit potential changed by less than 1 mV. The SOC studies were repeated until the electrode was discharged to its cutoff potential of −0.6 V. Cyclic voltammograms at different scan rates were obtained before and also after activating the electrode.

Results and Discussion

Discharge behavior.—Figure 2a presents the discharge curve for the cobalt-plated alloy after conditioning the electrode. The discharge curve for the bare alloy is also given for comparison. Initially the discharge is kinetically controlled, as indicated by the increase in the potential (E) to more positive values. As time proceeds the reaction is under mixed regime, with both diffusion and activation overpotentials controlling the rate of the reaction. For the cobalt-plated alloy the potential keeps changing slowly and rises drastically at −0.7 V. The potential again changes slowly and finally rises to the cutoff value of −0.6 V. This behavior is characteristic of electrodes on which two reactions are happening in succession. This discharge curve is unique to the cobalt-plated alloy and was not seen in the nickel, copper, palladium-plated, and bare alloy electrodes. Cobalt on the particle surface undergoes oxidation, contributing to an increase in the capacity of the electrode.[11,12] The change in the potential with time was gradual, which could be attributed to the oxidation of the cobalt coating during discharge. The additional faradaic

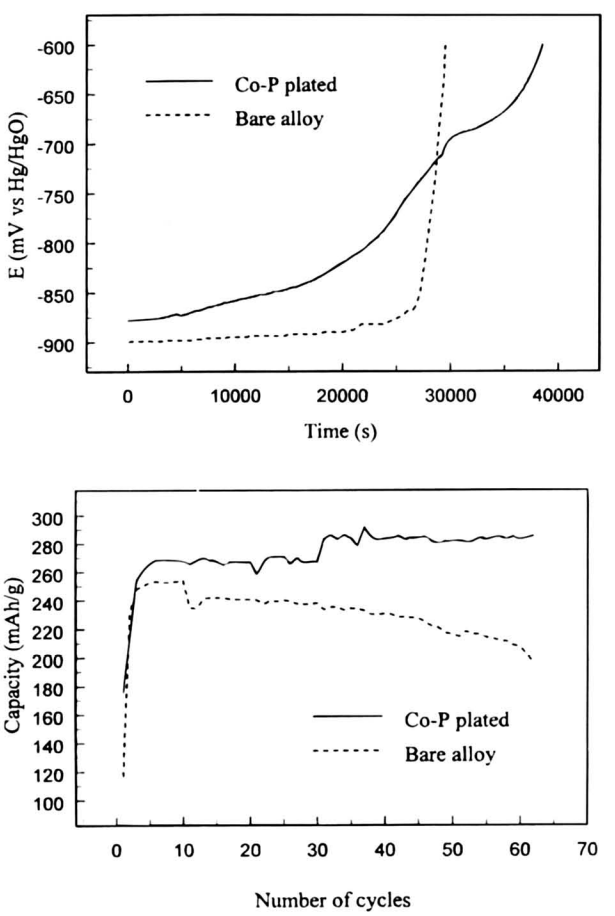

Fig. 2. Discharge curve of the cobalt-microencapsulated $LaNi_{4.27}Sn_{0.24}$ alloy in 6 M KOH. Two discharge profiles (a, top) arise due to the oxidation of cobalt on the surface and the desorption of hydrogen from the alloy. The total capacity due to these processes remains constant with cycling (b, bottom).

reaction due to cobalt oxidation was observed to occur at −0.7 V relative to the Hg/HgO reference electrode.

The discharge curves were highly repetitive and were observed during continuous cycles. Figure 2b presents the total capacity of cobalt-plated and bare $LaNi_{4.27}Sn_{0.24}$ alloy at different cycles. Microencapsulation with Co is seen to increase the capacity compared to the bare alloy. Also, the capacity of the cobalt-plated alloy remains constant during cycling, indicating that the oxidation products are reduced back to cobalt during the charging process. Recent studies on cobalt substitutions have indicated that it forms $Co(OH)_2$ on extended cycling.[10] The $Co(OH)_2$ is beneficial in improving the cycle life characteristics of the hydride electrode.

An added advantage of using cobalt shows in the high charge–discharge efficiencies observed for this electrode. Table I presents the time for charge and discharge for the cobalt-encapsulated alloy. After activation, it is seen that 100% charge efficiency is observed consistently. Since one of the problems associated with hydride alloys is overcharging, coating with Co seems to offer a way of achieving 100% efficiency. Further, after activation in all cycles the total time for discharge was slightly larger than that for charge. Higher utilization arises due to the cobalt oxidation mentioned before. In order to understand this phenomenon better we need to look at the equilibrium potential of the cobalt-plated alloy at different stages of discharge.

Equilibrium potential.—The open-circuit potential (E_{eq}) of the cobalt-plated electrode on immersion initially in the 6 M KOH solution is −0.75 V. Once the electrode is charged, the potential reaches more negative values because of the hydrogen intake. Using the three-electrode setup the constant equilibrium potential at different values of hydrogen content was measured with respect to the Hg/HgO reference electrode. Figure 3 presents the equilibrium potential of the bare and cobalt-plated $LaNi_{4.27}Sn_{0.24}$ at different SOCs. The potential values for the bare electrode do not vary much except at low and high SOCs.

The potential values of the cobalt electrode undergo a significant shift at 30% SOC. At high SOC the electrode is completely filled with hydrogen and the potential corresponds to the hydrogen electrode voltage. However, as hydrogen is depleted from the alloy the discharge curve given in Fig. 2a moves toward potentials at which cobalt oxidizes. In such a case, cobalt oxidation on the surface of the particle becomes the dominant faradaic reaction. The oxidation of cobalt in alkaline solutions results in the formation of $Co(OH)_2$, which is subsequently oxidized at more positive potential to higher oxides.[15] A dissolution–precipitation mechanism analogous to the anodic dissolution of iron in alkaline solution has been proposed by Popov et al.[15,16] for the $Co(OH)_2$ formation

$$Co + OH^- = CoOH_{ads} + e^- \quad [1]$$

$$CoOH_{ads} + OH^- = Co(OH)_{2,ads} + e^- \quad [2]$$

$$Co(OH)_{2,ads} + OH^- = HCoO_2^- + H_2O \quad [3]$$

Table I. Charge–discharge efficiency for the cobalt-encapsulated alloy at 0.1 C rate.

Number of cycles	Total time for charge (h)	Total time for discharge (h)	Charging efficiency (%)[a]
1	10	6:37	66.2
3	10	9:33	95.5
4	10	9:49	98.2
5	10	10:00	100
10	10	10:04	100.7
30	10	10:02	100.3
52	10	10:02	100.3

[a]Charging efficiency = $\frac{\text{Time for discharge}}{\text{Time for charge}} \times 100\%$.

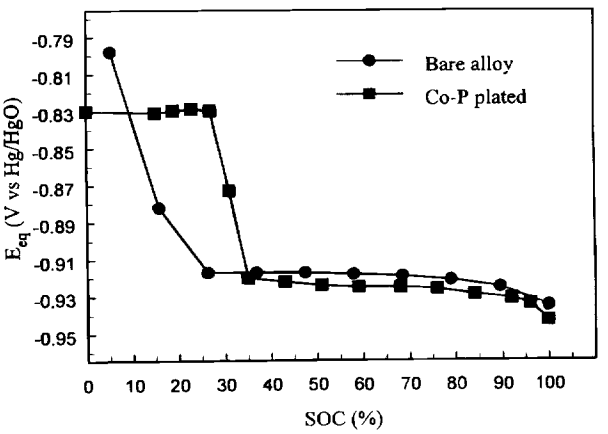

Fig. 3. Equilibrium potential vs. SOC for the $LaNi_{4.27}Sn_{0.24}$ electrode. A significant shift in the equilibrium potential at 30% SOC is seen for the cobalt-encapsulated alloy.

$$HCoO_2^- + H_2O = Co(OH)_2 + OH^- \quad [4]$$

The formation of $HCoO_2^-$ species is significantly low and hence the cobalt electrode potential is controlled by the $Co/Co(OH)_2$ couple. In order to understand the cobalt reaction mechanism, potential sweep techniques covering a wide range of scan rates were performed.

Cyclic voltammograms.—The cyclic voltammetry (CV) behavior of the pellet electrode at different scan rates is illustrated in Fig. 4 and 5. Figures 4 and 5 present the CVs before and after activation, respectively. The potential (E) was varied from −0.5 to −1.2 V in both directions and the current (I) response was measured in succession for different scan rates. The potential range of −0.5 to −1.2 V represents the stable region for the alloy $LaNi_{4.27}Sn_{0.24}$ where the material is not oxidized. The pellet adsorbs and desorbs hydrogen and acts as a reversible electrode with respect to hydrogen. Hence, the voltammograms can be viewed from the point of charging and discharging the electrode by varying the current through the potential. Such an approach allows us to interpret the unique features of a CV, namely, the appearance of maxima in the current during the voltage sweep and the potential at which this peak occurs. We first present CVs at high scan rates in Fig. 4 and 5a. The CVs at low sweep rates are presented in Fig. 5b. The open-circuit potential of the cobalt-plated electrode initially on immersion in 6 M KOH is −0.75 V. Hence, decreasing the potential toward more negative values from −0.5 V results in oxidizing the cobalt on the electrode surface. Beyond −0.75 V cobalt is reduced.

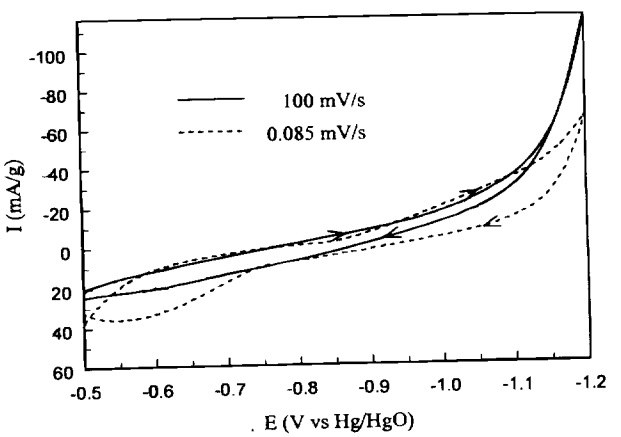

Fig. 4. Cyclic voltammograms of the cobalt-plated alloy performed before activating the pellet electrode. The sweeps were done in succession starting at −0.5 to −1.2 V and then back to −0.5 V.

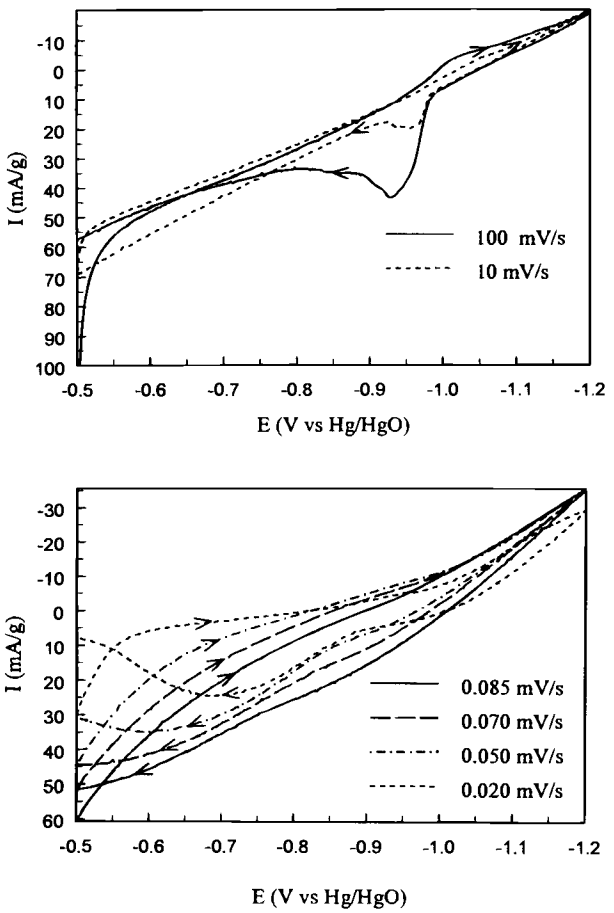

Fig. 5. Cyclic voltammograms of the cobalt-encapsulated alloy after activation. At high scan rates (a, top) hydrogen adsorbed in the cobalt film on the particle surface is desorbed. At low sweep rates (b, bottom) cobalt is oxidized and subsequently hydrogen is desorbed.

Further decreasing the potential results in hydrogen absorption in the alloy particle. The currents for these two processes are negative, indicating that different species are reduced on the electrode surface. The current maximum observed at −1.2 V corresponds to the limit of the hydrogen evolution reaction on the hydride electrode. Similar results are seen in Fig. 5a after conditioning the electrode.

However, in the reverse sweep peaks appear which become smaller with a decrease in the scan rate. These peaks are not observed in Fig. 4 before activating the electrode. The appearance of these peaks is associated with the cathodic activation of the electrode with charge–discharge cycling. The CVs in Fig. 5a were done after completely charging the electrode, which corresponded to cathodically activating the electrode for approximately 12 h. Similar results were seen by Popov et al.[15,16] in their studies on cobalt in 1 M NaOH solution. After long cathodic activation (20 min and more) at −1.5 V vs. SCE, shoulders appeared before the oxidation peak of cobalt in their voltammograms. These shoulders were absent when the electrode was not cathodically pretreated. They concluded that the appearance of the shoulder was due to the anodic oxidation of hydrogen adsorbed in cobalt.[16] Since cathodic activation in our case was for 12 h, significant peaks are seen as compared to the appearance of shoulders.[16] However, at successive sweeps the hydrogen adsorbed in the cobalt gets depleted and the magnitude of the peaks becomes progressively smaller until it completely disappears at a scan rate of 0.2 mV/s. By integrating the area under the peak at 10 mV/s we got the amount of charge from the oxidation of adsorbed hydrogen as 0.183 mAh/g.

By lowering the rate at which the system is perturbed from equilibrium, the hydrogen concentration gradient at the particle surface is increased. In these CVs we are not lowering the amount of perturbation from equilibrium but rather the rate at which the system is perturbed from equilibrium. At all scan rates the perturbation from equilibrium is the same, i.e., shifting the potential from −0.5 to −1.2 V and then back to −0.5 V. The kinetic rate remains the same at all potential values for these CVs. For example, when the potential is at −0.5 V, the kinetic rate is the same irrespective of whether the potential is swept at 100 mV/s or 0.02 mV/s. However, the current which depends on the mass transfer and ohmic limitations apart from the reaction kinetics is different. Since the ohmic losses are the same for all sweep rates, we focus our attention on the effect of mass transfer. Generally, in electrochemical systems, mass-transfer limitations are in the solution and outside the particle. However, in the case of metal hydrides, the mass-transfer limitation arises due to the diffusion of hydrogen inside the particle. There is no boundary layer in this case. However, a diffusion layer does exist between the surface and the next layer of hydrogen atoms in the particle.

Under such conditions we look at the case of very fast reaction kinetics. This would be at −0.5 V, since maximum perturbation of potential from equilibrium happens here. At high scan rates the time for which the potential is kept at −0.5 V (corresponding to very fast reaction kinetics) is small. In such an instance, hydrogen is depleted at the surface and this forces the diffusion of hydrogen to the particle surface. However, not all the hydrogen at the surface is depleted, since the large currents are applied for a small period of time only. The concentration difference between the surface and the adjacent layer of hydrogen atoms is small. Hence, the gradient is small and the current is also low. However, at low scan rates the time at which the potential is kept at −0.5 V (fast reaction kinetics) is very large. This depletes most of hydrogen from the surface of the particle. Hence, the difference in concentration in hydrogen between the surface and the next layer of atoms is very large. Therefore, both the concentration gradient and the current are also large. The rise in the current and subsequent fall is due to the "relaxation effect" seen in conventional voltammograms. The concentration gradient is at its maximum when the surface concentration drops to zero. If the material is discharged beyond this point hydrogen is progressively depleted from the adjacent layers to the surface. Due to this, the diffusion layer thickness, which is the difference between the surface and the next layer of hydrogen atoms, widens. This leads to a drop in the concentration gradient and hence the current, even though the concentration difference is at its maximum. Hence, the maxima in the peaks increases when the scan rate is decreased.

From Fig. 2a we can see that the second discharge plateau corresponding to the oxidation of cobalt begins at −0.7 V. As seen from Fig. 3, the potential of the electrode at low SOC is controlled by the $Co/Co(OH)_2$ couple. Hence the maximum and subsequent relaxation seen in Fig. 4 and 5b involves two electrochemical reactions, namely, desorption of hydrogen and also the oxidation of cobalt. As seen in Fig. 5b, after activation more hydrogen is present in the electrode and hence the anodic currents are significantly higher. Before activation the encapsulated alloy behaves similar to the bare electrode and the peak appears close to −0.6 V. However, the appearance of the peak is shifted toward more negative potential after conditioning due to the prolonged cathodic activation. This shift in the electrode potential is discussed in detail later in this paper. The total currents for charging and discharging the electrode have been integrated and are presented in Table II for both before and after activating the electrode. Net amount of charge expended (charge–discharge) was toward charging the electrode (−67 mAh/g) for the unactivated alloy, whereas for the other case more charge was spent on discharge (+302 mAh/g). Since the CVs were performed from a very negative potential (−0.5 V) as compared to the open-circuit value (−0.936 V), the electrode

Table II. Total charge passed during potential sweep studies of the cobalt-encapsulated electrode.

Scan rate (mV/s)	Q_a (mAh/g)		Q_c (mAh/g)	
	Initial	Activated	Initial	Activated
10	0.16	1	0.43	0.09
1	1.5	9	3.6	0.9
0.5	3	20	6.4	2
0.2	8	55	14	9
0.1	23	89	26	19
0.085	37	78	40	26
0.07	43	77	52	34
0.05	58	83	69	50
0.02	107	118	136	89
Net charge	280	532	347	229

remained in the discharge mode for a longer period of time for the conditioned alloy.

Figure 6 presents the CVs at a scan rate of 0.02 mV/s. The first curve corresponds to the voltammograms measured after activating the electrode (as presented in Fig. 5b). The second CV was taken immediately after charging the electrode. Two peaks are seen in this case during the reverse sweep corresponding to the two plateaus observed in the discharge curve of Fig. 2a. The first peak is due to the desorption of hydrogen from the alloy and the second one corresponds to the oxidation of cobalt from the surface of the particle. As shown in Fig. 5b, the CVs were done in succession and hence most of the cobalt was oxidized before a scan rate of 0.02 mV/s reached. Hence, the current was a combination of both electrochemical reactions and a single broad peak is seen. However, when the CV is done immediately after charging the electrode, these reactions are seen separately as two distinct peaks. In order to understand the process associated with cobalt, thin films of cobalt were prepared and studied in isolation.

Thin-film studies.—Thin films of cobalt were deposited on a platinum disk electrode of area 0.5 cm^2. The deposition procedure is the same as described previously for microencapsulation of the alloy. The deposited films were then studied in 6 M KOH using nickel as the counter electrode and Hg/HgO as the reference electrode. To prevent the evolution of hydrogen on the electrode, the maximum applied negative potential was −1.0 V for all the studies. The cyclic voltammograms of a thin film of cobalt deposited on a platinum disk electrode with potential scanned from −1.0 V is illustrated in Fig. 7. As the potential is shifted to more positive values, cobalt is oxidized to

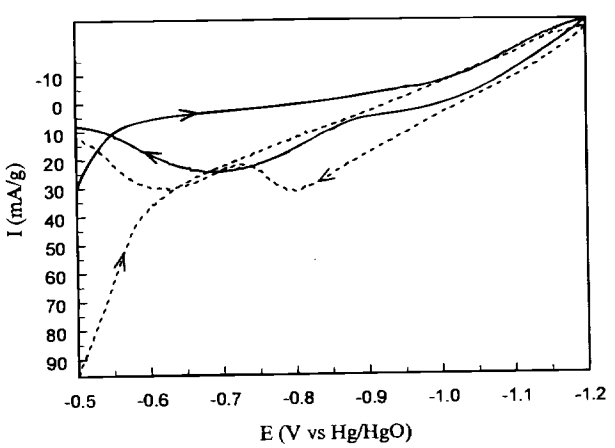

Fig. 6. Voltammograms of the cobalt-plated alloy at a scan rate of 0.02 mV/s. The solid line shows the CV at 0.02 mV/s given in Fig. 5b where the potential was swept at different scan rates in succession. Separately, the electrode was charged and the current–potential response was measured immediately at a sweep rate of 0.02 mV/s, which is given by the dashed line.

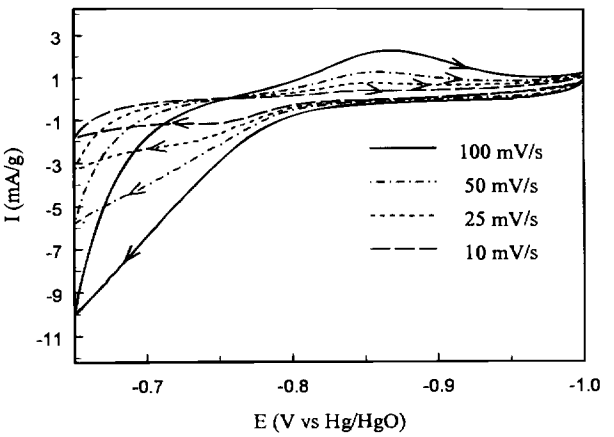

Fig. 7. CVs of the thin film at different sweep rates in 6 M KOH. The film was deposited under conditions similar to the microencapsulation of cobalt on the alloy.

$Co(OH)_2$. This is seen from the increase in the current beyond −0.8 V. On the reverse scan a peak is observed at −0.86 V corresponding to the reduction of the oxides to cobalt. The appearance of these reaction peaks is discussed in detail later in this paper. The magnitude of both peaks depends on the scan rate, and with increasing sweep rates, the peak height also increases. However, for all sweeps the forward anodic peak has a greater magnitude as compared to the reverse cathodic peak. This indicates that the rate of oxidation is more compared to the rate of reduction. Hence, prolonged cathodic activation is essential to reduce all the oxides to cobalt.

In order to study the effect of cathodic reduction on cobalt, the film is stripped and cobalt deposition is done again under similar conditions on Pt. The film is then polarized at −1.0 V in 6 M KOH (similar to the electrolyte used in the charge–discharge studies for the pellet electrode) for 15 min. Figure 8 presents the voltammograms at different scan rates for the treated film. Apart from the peaks for the oxidation of cobalt, a broad shoulder appears for all sweep rates starting at −0.75 V. These features are absent for the film before the cathodic treatment, as illustrated in Fig. 7. The fact that it is necessary to apply a long activation at −1.0 V to observe the peak at −0.75 V suggests that this shoulder is due to adsorbed hydrogen in Co rather than to the formation of adsorbed CoOH species as suggested by Meier et al.[17] and Novoseleskii and Menglisheva.[18] The hydrogen adsorbed is subsequently oxidized when the potential is swept to more anodic values. Further, the magnitude of the peaks increases with increase in sweep rate. These results are in

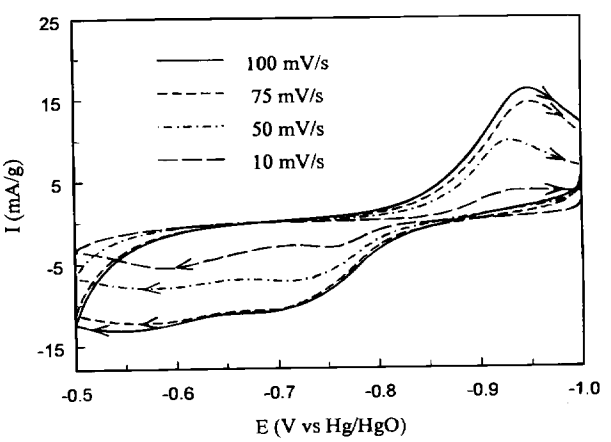

Fig. 8. CVs of the thin film in 6 M KOH solution after cathodic treatment. The cobalt film was kept at −1.0 V in 6 M KOH for 15 min.

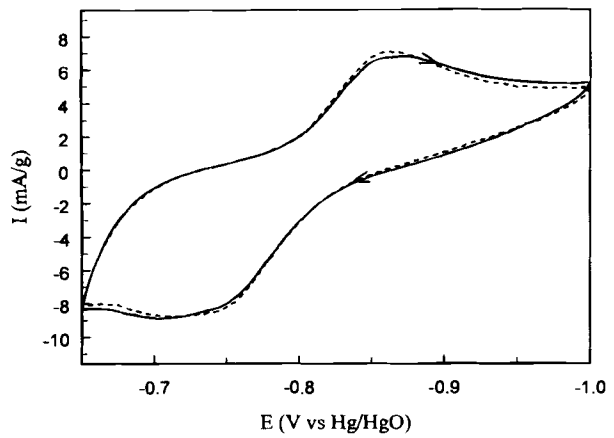

Fig. 9. CVs of the cobalt film at 100 mV/s in 6 M KOH solution. The solid line shows the voltammogram after the first cycle and the dashed line presents the current response after 50 cycles.

agreement with the sharp peaks observed for the cobalt-plated electrode at high scan rates as shown in Fig. 5a.

Figure 9 shows the effect of cycling the film between −1.0 and −0.65 V at a scan rate of 100 mV/s. The capacity after cycling 50 times remains the same and the film behavior is highly consistent.

Figure 10a presents the CVs of the cobalt film between −1.0 and −0.8 V at 100 mV/s. Since the potential was not taken below −0.8 V, cobalt is not oxidized. This results in the absence of reduction peaks observed during the reverse sweeps in Fig. 7 and 8. This is more clearly illustrated in Fig. 10b where the potential was scanned at 100 mV/s from −1.0 V to different end potentials, namely, −0.75, −0.7, −0.65, −0.6, −0.55, and −0.5 V in succession. Each of these CVs were repeated five times and the 5th cycle is presented for all cases. As the potential is shifted toward more positive values, more amount of cobalt is oxidized. Hence, for a particular sweep rate of 100 mV/s, this results in increasing the reduction peak current. As seen from the plot, when the potential is shifted behind −0.6 V, the anodic oxidation current decreases, indicating that the oxides formed during the anodic cycle are not reduced completely at potentials more negative than −0.85 V. However, the amount of cobalt oxidized is significant enough to account for the increase in the reduction current for all cases.

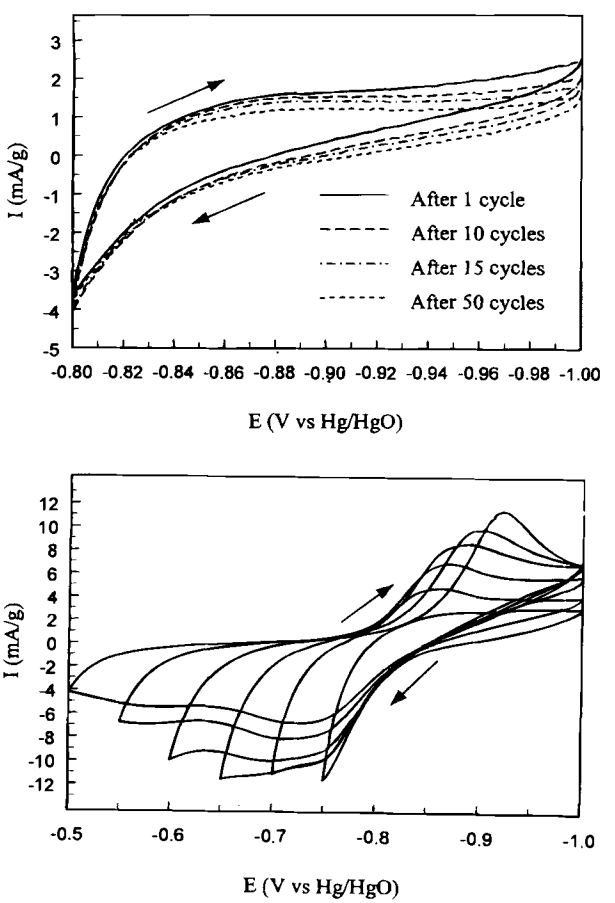

Fig. 10. CVs of the cobalt film at 100 mV/s in 6 M KOH. The hydrogen desorption peaks seen in Fig. 7 are absent when the potential is not shifted beyond −0.8 V (a, top). As the potential is swept to more negative values (b, bottom) the cathodic reduction peaks of cobalt increase in magnitude.

The amount of hydrogen adsorbed in the film is investigated further by cathodically polarizing a freshly prepared film in 6 M KOH solution. Figure 11 presents the open-circuit potential of the thin cobalt film as a function of time after cathodic treatment for different time periods. The initial potential of the cobalt film after immersion in 6 M KOH solution is −0.83 V. The film is polarized at −1.0 V for 5 s and the potential is then monitored continuously. The same film was polarized for 15 s and the open-circuit potential was subsequently studied. Similar studies after polarization were done for 25, 50, 120, 300, 600, 900, and 1200 s. As shown in the plot, after polarizing the film the potential shifts toward more negative values due to the adsorption of hydrogen in the film. This potential should be considered as a hydrogen electrode "floating potential" whose value depends not only on the amount of hydrogen adsorbed in Co but also on the local concentration of dissolved hydrogen formed during the activation process. As the electrode is polarized for longer periods of time, more hydrogen is adsorbed and the potential becomes closer to the hydrogen electrode voltage. However, beyond 1200 s of polarization, the potential does not change significantly, indicating that the hydrogen adsorbed is at its maximum value. Potential decay curves shown in Fig. 11 can be explained by taking into account the fact that as time proceeds, the hydrogen adsorbed in Co diffuses out and the electrode potential becomes more positive. The observed leveling of the potential indicates that the open-circuit potential becomes controlled by the Co electrode reactions (Eq. 1-4).

The oxidation of hydrogen is investigated by polarizing a separate film at −1.0 V for 180 s. The potential is then shifted to −0.7 V so that the entire amount of adsorbed hydrogen is oxidized. This is seen by monitoring the current, which decays rapidly to zero once the hydrogen is oxidized. Similar studies were done by polarizing the film for 300 and 420 s. Table III presents the net amount of

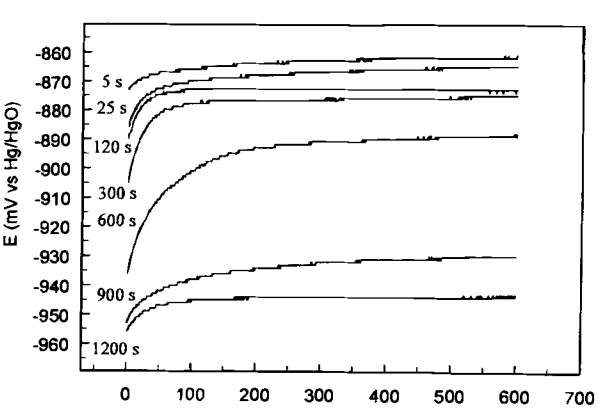

Fig. 11. *E* vs. *t* curves of the cobalt film after cathodic polarization at −1.0 V in 6 M KOH for different times. The potential shifts to more negative values because of the increase in the adsorbed hydrogen.

Table III. Net charge passed during cathodic activation and anodic oxidation of cobalt film.

Time of cathodic activation (s)	Cathodic charge (mC)	Anodic charge (mC)
180	−185.3	+177
300	−308.7	+288
420	−362.9	+315

charges passed during both the cathodic activation at −1.0 V and also the anodic oxidation at −0.7 V. It can be seen that the net charges of reduction and oxidation correspond closely with each other. These results indicate that the hydrogen present in the cobalt film exists in a loosely adsorbed state and can be easily oxidized.

Exchange current density.—At low overpotentials, linearization of the Butler–Volmer equation results in

$$R_{ct} = \frac{RT}{F}\frac{1}{j_o} = \frac{\eta}{i} \qquad [5]$$

Here the charge-transfer resistance denoted by R_{ct} is the slope of the current–potential lines presented in Fig. 12. The extent of change in the electrode potential with current, i.e., the polarizability, is characterized by the slope, R_{ct}. The polarization resistance shows a significant decrease when the SOC decreases, indicating that the hydrogen desorption reaction occurs much more easily on the Co surface. The shift in the *E-i* curves seen in Fig. 12 agrees with the change in the equilibrium potential shown in Fig. 3. The exchange current densities (I_o) for the bare and cobalt-plated electrode are summarized in Fig. 13 as a function of electrode hydrogen content. In Fig. 13 we observe that the exchange current density of the bare alloy varies significantly with SOC. For the cobalt coatings the j_o values remain constant throughout and vary slightly only at low and high SOC. However, it can be seen that the cobalt coating significantly reduces the rate of hydrogen desorption at the surface of the alloy. This would affect the high-rate discharge characteristics of the hydride electrode.

Conclusions

$LaNi_{4.27}Sn_{0.24}$ alloy was microencapsulated with 28 wt % cobalt from an alkaline hypophosphite bath. Studies show that cobalt has several advantages over other electroless coatings for the microencapsulation of metal hydrides. First, the encapsulation results in an adherent magnetic deposit with greater ease in preparation of pellet electrodes. Second, discharge curves of the electrode reveal an additional faradaic contribution from the cobalt microencapsulation. Cyclic voltammograms of the activated electrode reveal diffusion-limited hydrogen desorption peaks and also the faradaic cobalt reaction peaks during the reverse sweep at low scan rates. The magnitude of the peaks increased with a decrease in the scan rate. The CVs were analyzed from the point of charge–discharge curves, i.e., positive and negative currents correspond to discharging and charging the electrode, respectively. Third, apart from the faradaic reaction, cobalt also adsorbs hydrogen, which contributes to the capacity. For the fully conditioned electrode, peaks were observed in the reverse scan at high sweep rates. Studies on thin cobalt films show that these peaks correspond to the hydrogen adsorbed in the film during cathodic polarization. Increasing the time of polarization resulted in more hydrogen being adsorbed. Further, CVs on the film reveal that the cobalt oxidized during the anodic process is reduced during the reverse sweep. However, since the rate of reduction is lower than that of oxidation, prolonged cathodic treatment is essential to reduce all the oxides to cobalt. The charging efficiency of the cobalt-encapsulated alloy is close to 100% due to these processes. Electrochemical characterization studies were performed on the cobalt-plated electrode at different SOCs. The equilibrium potential was found to be closely dependent on the hydrogen content in the electrode. Up to 30% SOC the alloy behaved as a cobalt electrode and at higher SOC values the potential shifted to the hydrogen electrode voltage.

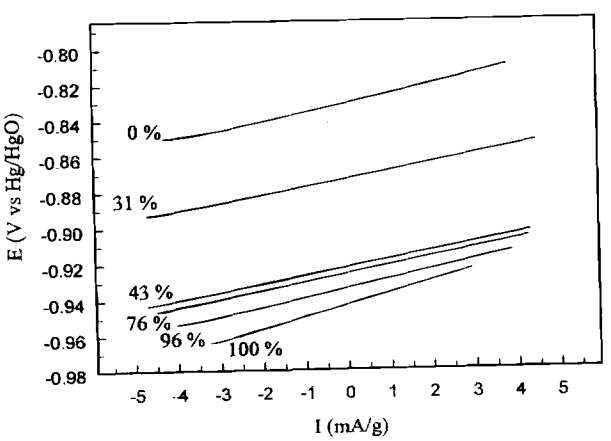

Fig. 12. Current–potential curves for the cobalt-encapsulated alloy at different SOCs. The slope of the *E-I* lines gives the polarization resistance (R_p).

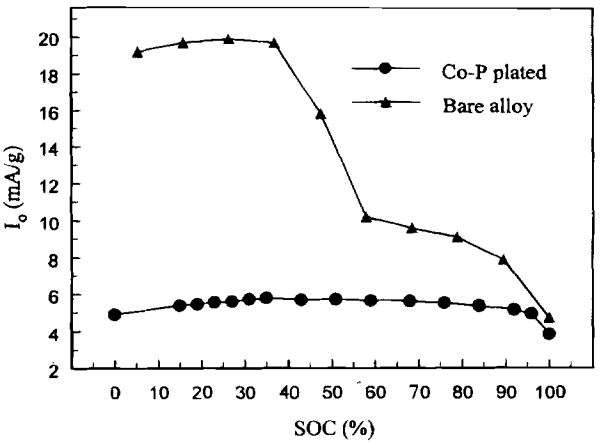

Fig. 13. Exchange current density of the $LaNi_{4.27}Sn_{0.24}$ electrode at different SOCs. The exchange current is calculated from the polarization resistance (R_p) as given by Eq. 5.

Acknowledgment

Financial support by the Exploratory Technology Research (ETR) Program, which is supported by the Office of Transportation Technologies (OTT) of the U.S. Department of Energy (DOE), subcontract no. 4614610, is gratefully acknowledged.

Manuscript submitted November 20, 1997; revised manuscript received May 7, 1998.

The University of South Carolina assisted in meeting the publication costs of this article.

REFERENCES

1. T. H. Fuller and J. Newman, in *Modern Aspects of Electrochemistry*, Vol. 27, J. O'M. Bockris, B. E. Conway, and R. E. White, Editors, p. 359, Plenum Press, New York (1993).
2. H. F. Bittner and C. C. Badcock, *J. Electrochem. Soc.*, **130**, 193C (1983).
3. L. Schlapbach, A. Seiler, H. C. Siegmann, T. V. Waldkrich, and P. Zurcher, *Int. J. Hydrogen Energy*, **4**, 21 (1979).
4. Y. Q. Lei, Z. P. Li, C. P. Chen, J. Wu, and Q. D. Wang, *J. Less-Common Met.*, **172-174**, 1265 (1991).
5. T. Sakai, H. Ishikawa, K. Oguro, C. Iwakura, and H. Yoneyama, *J. Electrochem. Soc.*, **134**, 558 (1987).
6. K. Naito, T. Matsunami, K. Okuno, M. Matsuoka, and C. Iwakura, *J. Appl. Electrochem.*, **24**, 808 (1994).

7. S. N. Jenq, H. W. Yang, Y. Y. Wang, and C. C. Wan, *J. Power Sources*, **57**, 111 (1995).
8. G. Zheng, B. N. Popov, and R. E. White, *J. Electrochem. Soc.*, **143**, 834 (1996).
9. T. Sakai, H. Yoshinaga, H. Miyamura, N. Kuriyama, and H. Ishikawa, *J. Electrochem. Soc.*, **180**, 37 (1992).
10. D. Chartouni, F. Meli, A. Zuettel, K. Gross, and L. Schlapbach, *J. Alloys Compd.*, **241**, 160 (1996).
11. T. Weizhong, G. Yingxin, and Z. Haoyu, *J. Appl. Electrochem.*, **25**, 874 (1995).
12. C. Iwakura, Y. Fukumoto, M. Matsuoka, T. Kohno, and K. Shinmou, *J. Alloys Compd.*, **192**, 152 (1993).
13. T. Ikeya, K. Kumai, and T. Iwahari, *J. Electrochem. Soc.*, **140**, 3082 (1993).
14. G. G. Gawrilov, *Chemical Nickel Plating*, Portcullis Press, Ltd., Surrey, England (1979).
15. B. N. Popov, Z. Koneska, J. Ivshin, and D. M. Drazic, *J. Serb. Chem. Soc.*, **54**, 435 (1989).
16. B. N. Popov, Z. Koneska, J. Ivshim, and D. M. Drazic, *J. Serb. Chem. Soc.*, **54**, 443 (1989).
17. H. G. Meier, J. R. Vilche, and A. J. Arvia, *J. Electroanal. Chem.*, **134**, 251 (1982).
18. I. M. Novoseleskii and N. R. Menglisheva, *Electrochim. Acta*, **29**, 21 (1984).
19. T. Sakai, K. Oguro, H. Miyamura, N. Kuriyama, A. Kato, and H. Ishikawa, *J. Less-Common Met.*, **161**, 193 (1990).
20. L. Schlapbach, A. Seiler, F. Stucki, and H. C. Siegmann, *J. Less-Common Met.*, **73**, 145 (1980).
21. T. Sakai, H. Ishikawa, K. Oguro, and C. Iwakura, *Prog. Batteries. Sol. Cells*, **6**, 221 (1987).

Shape Evolution of Electrodeposited Bumps with Deep Cavity

Kazuo Kondo*,[a] and Keisuke Fukui[b]

[a]*Faculty of Engineering, University of Okayama, 3-1-1 Tushima-Naka, Okayama 700, Japan*
[b]*Faculty of Engineering, Himeji Institute of Technology, Shosha, 2167, Himeji 671-22, Japan*

ABSTRACT

Electrodeposited bumps are the indispensable microconnectors for high-density interconnection in the latest microelectronics applications. The deep cavities are especially important for the solder bumps for ball grid arrays. This investigation discusses the relation between cavity shapes and current distributions of deep cavities. The role of convection and diffusion within the cavities is calculated at diffusion-limited overpotentials with numerical fluid dynamics computations. The current distributions become symmetric and peak profiles become sharper for the deeper cavities of large aspect ratios and of negative photoresist angles, θ. For 30 μm cathode length, the current at the center is larger than that at the edges for photoresist angles of $\theta \leqq 0$. For these deep cavities, the convection outside the cavity is not related to the current distribution and the current distribution is determined by the cavity shape. The mass transport within the deep cavities is controlled mainly by diffusion. This is because the convection outside the cavities is not effectively stirring inside the deep cavities.

Introduction

Electrodeposited bumps are the indispensable microconnectors for high-density interconnection in the latest microelectronics applications.[1] For the higher frequency circuit, shorter interconnection length by bumps is required in order to reduce the reflection noise. Most conventional application is the interconnection between liquid crystal display (LCD) and driver chips, which are mostly interconnected with tape-automated bonding (TAB).[2] Recently, ball grid array (BGA) of solder bumps has become necessary for high-pin-count chips in order to reduce their packaging size. These solder bumps are formed within the deep cavities.

The bumps are electrodeposited onto the dot-shaped cathode several 10s to 200 μm diam. The cathode, or photolithography patterns, are patterned by photomask and photoresist. The current distribution problems for bumping are extensively discussed by several authors. Dukovic developed two-dimensional numerical computation of tertiary current distribution only including the diffusion. The moving boundary problem was discussed on shape evolution of copper electrodeposit and the effect of resist wall angle and leveling agent was reported.[3] Leyerdecker et al.[4] discussed the mass transport for deep cavities of the LIGA process and referred to the importance of diffusion. The experimental studies on shape evolution of gold bumps were discussed by Kondo et al.[5] We studied the effects of dot diameter, electrolyte flow, and additive on bump shapes. The numerical fluid dynamics computation study on initial stage of gold and copper bumps at a lower Peclet number of less than 100 were reported.[6,7] We further reported the numerical fluid dynamics computation study of copper bumps at higher Peclet numbers more than 100.[8] Recently, we studied the shape evolution of copper bumps with photoresist angles.[9]

This investigation discusses the cavity shapes and the current distributions for deep cavities. The role of convection and diffusion within the cavities is discussed. The current distributions at diffusion limited overpotentials were calculated by the numerical fluid dynamics computations.

Numerical Analysis

Fluid flow-field and concentration profiles are numerically analyzed by solving the equation of continuity, Navier–Stokes equations, and mass-transfer equation

$$\frac{\partial u}{\partial x} + \frac{\partial v}{\partial y} = 0 \qquad [1]$$

$$\rho\left(u\frac{\partial u}{\partial x} + v\frac{\partial u}{\partial y}\right) = -\frac{\partial p}{\partial x} + \mu\left(\frac{\partial^2 u}{\partial x^2} + \frac{\partial^2 u}{\partial y^2}\right) \qquad [2]$$

$$\rho\left(u\frac{\partial v}{\partial x} + v\frac{\partial v}{\partial y}\right) = -\frac{\partial p}{\partial y} + \mu\left(\frac{\partial^2 v}{\partial x^2} + \frac{\partial^2 v}{\partial y^2}\right) \qquad [3]$$

$$u\frac{\partial c}{\partial x} + v\frac{\partial c}{\partial y} = D\left(\frac{\partial^2 c}{\partial x^2} + \frac{\partial^2 c}{\partial y^2}\right) \qquad [4]$$

The computational configuration and the boundary conditions with resist angle θ are illustrated in Fig. 1. The resist angle θ is not equal to zero. We discretized these equations using a nonorthogonal coordinate system[10] in order to generate the boundary-fit grids. The numerical computations were performed using a conservation finite volume method with a colocated variable arrangement provided by Peric.[11] The velocity components and the pressure are linked with the SIMPLE algorithm of Patanka.[12] Copper electrodeposits

* Electrochemical Society Active Member.